UNIVERSITY OF CALIFORNIA, MERCED

Title

Biophysical Analysis of Anti-Inflammatory Viral CC Chemokine Binding Protein vCCI

A dissertation submitted in partial satisfaction of the

requirements for the degree of

Master of Science

in

Chemistry and Chemical Biology

by

Laura Janelle Showalter

Committee in charge:

Professor Michael Colvin, Chair of Advisory Committee

Professor Eva de Alba Bastarrechea

Professor Maria Zoghbi

Professor Patricia LiWang, Supervisor

2018

The dissertation of Laura Janelle Showalter, titled, “Biophysical Analysis of Anti-Inflammatory Viral CC Chemokine Binding Protein vCCI”, is approved, and is acceptable in quality and form for publication on microfilm and electronically:

_____ Date _____

Professor Eva de Alba Bastarrechea

_____ Date _____

Professor Maria Zoghbi

Supervisor _____ Date _____

Professor Patricia J. LiWang

Chair _____ Date _____

Professor Michael Colvin

University of California, Merced

2018

Dedications

I dedicate this work to my family, best friends, and significant other. They have been so supportive and understanding of my having very little time to spend with them to accomplish this body of work. Those who want the best for you, celebrate successes with you, and lend an ear during difficult times make life so incredibly richer. I will never stop appreciating how much they all add to my life.

Table of Contents

I. List of Abbreviations

aa	Amino Acid
Acn	Acetonitrile
bp	Base Pair
CCR5	CC Chemokine Receptor Type 5
Conc	Concentration
CXCR4	CXC Chemokine Receptor Type 4
DNA	Deoxyribonucleic Acid
dNTP	deoxyriboNucleotide TriPhosphate
DSS	NMR Standard, 4,4-dimethyl-4-silapentane-1-sulfonic acid
EDTA	Ethylenediaminetetraacetic acid, also known as 2-[2-[bis(carboxymethyl)amino]ethyl-(carboxymethyl)amino]acetic acid
EK	Enterokinase
GSH	Reduced glutathione
GSSG	Oxidized glutathione
HIV	Human Immunodeficiency Virus
HSQC	Heteronuclear Single Quantum Coherence
IPTG	Isopropyl β-D-1-thiogalactopyranoside
KCl	Potassium Chloride
K_D	Dissociation Constant
kDa	Kilodaltons
KPi	Potassium Phosphate
L-Arg HCl	L-Arginine hydrochloric acid
MD	Molecular Dynamics
MIP-1α	Macrophage Inflammatory Protein 1 alpha, also known as CCL3 (CC Chemokine Ligand Type 3)
MIP-1β	Macrophage Inflammatory Protein 1 beta, also known as CCL4 (CC Chemokine Ligand Type 4)
MWCO	Molecular Weight Cut Off
NaCl	Sodium Chloride

NaOAc	Sodium Acetate
NaPi	Sodium Phosphate
NEB	New England Biolabs
NMR	Nuclear Magnetic Resonance
Nt	N-terminal
OD_{600}	Optical density (measured with a UV-Vis spectrophotometer) at 600 nm
Oligo	Oligonucleotide
PCR	Polymerase Chain Reaction
Pol	Polymerase
RANTES	Common name for CCL5 (CC Chemokine Ligand Type 5)
SAP	Shrimp Alkaline Phosphatase
SDS-PAGE	Sodium Dodecyl Sulfate - PolyAcrylamide Gel Electrophoresis
SEC	Size Exclusion Chromatography
SPR	Surface Plasmon Resonance
SUMO	Small Ubiquitin-like Modifier
Taq	Thermus aquaticus (a thermophilic bacterium)
TFA	Trifluoroacetic Acid
Tm	Melting Temperature
Tris	Tris(hydroxymethyl)aminomethane, also known as 2-Amino-2-(hydroxymethyl)-1,3-propanediol
Txn	Thioredoxin
UC Berkeley	University of California, Berkeley
UC Merced	University of California, Merced
UV-Vis	Ultraviolet-visible spectroscopy
vCCI	Viral CC Chemokine Inhibitor
vMIP-II	Viral Macrophage Inflammatory Protein - II
WT	Wild Type
βME	2-Mercaptoethanol

II. List of Figures

Chapter 1 Figures:

Chapter 2 Figures:

Chapter 3 Figures:

III. List of Tables

Chapter 1 Tables:

Chapter 2 Tables:

Chapter 3 Tables:

IV. Acknowledgments

There is a long list of people who have given me knowledge, perspective, experience, advice, and support. First of all, I would like to thank my advisor, Prof. Patti LiWang, for the opportunity to join her lab as an undergraduate originally and to continue working with her as a staff research technician and then as a master's student. I have learned so much in a knowledge-based and technical sense, but perhaps even more in a personal sense. The opportunity she gave me was my first research experience and I enjoyed it so much, it altered the course of my future, culminating in my decision to pursue research as a career. I am incredibly grateful for the time, energy, and resources she poured into me to help shape me into the scientist I am today.

The first mentor I had in Patti's Group was Mike Jian. He taught me many of the foundational techniques and the importance of challenging myself to seek out the 'why' behind the methods and instruments I use. Dr. Li Zhang added to this. He made me think deeply and imprinted the need to be hyper-careful with lab work and have excellence in the ordinary so that I could get more meaningful results. Thank you to Anna Faith Nguyen for the mentorship you gave me. Other members of both the Patti and Andy LiWang Groups helped me along the way as well. Thank you to Dr. Archana Chavan for teaching me how to use the ITC instrument and always being willing to discuss experiments with me. I appreciate Arjan Bains' willingness and excitement to discuss research results with me. Additionally, thank you to recently graduated Mina Tawfick for his help with preparing for experiments.

There are several professors who have had a big impact on me as well. I am forever grateful to Prof. Mike Colvin for the knowledge and perspectives he has instilled in me, his support, and for serving as the chair of my committee. It has been an absolute pleasure to work with you in both teaching and our research collaboration. Thank you to Prof. Maria Zoghbi and Prof. Eva de Alba for serving on my committee and for your advice. I would like to thank both Prof. David Kelley and Prof. Andy LiWang for teaching powerful and often underrated common sense in the classes I have taken with you. It has had a large impact on my thinking. I am also grateful for your time in discussing all matter of other things relating to research, career, and beyond. Thank you to Prof. Shahar Sukenik for teaching me about CD, how to use the instrument, and for his assistance in processing data.

Lastly, there are other professors that have had a large impact on me throughout my UC Merced tenure, including Christine Isborn, Alex Whalley, and Justin Hicks. Thank you to all for your support and the opportunities you gave me.

V. Vita for Laura Janelle Showalter

Education:

University of California, Merced **01/2018 – 12/2018**
Chemistry and Chemical Biology, M.S.

University of California, Merced **08/2013 – 05/2016**
Chemical Sciences, B.S. and Management, B.S.
Graduated with Highest Honors

List of Publications:

Burcin Yavuz, Jessica L. Morgan, **Laura Showalter**, Katti R. Horng, **2018**
Satya Dandekar, Carolina Herrera, Patricia LiWang*, and David L. Kaplan*
Pharmaceutical Approaches to HIV Treatment and Prevention
Advanced Therapeutics, doi: 10.1002/adtp.201800054

Anna F. Nguyen, Nai-Wei Kuo, **Laura J. Showalter**, Ricardo Ramos, **2017**
Cynthia M. Dupureur, Michael E. Colvin and Patricia J. LiWang*
Biophysical and Computational Studies of the vCCI:vMIP-II Complex
International Journal of Molecular Sciences, 18(8), 1778

Awards and Fellowships:

Outstanding Student in Chemistry & Chemical Biology at UC Merced **2016**
UC Merced Natural Sciences and Engineering Commencement Speaker **2016**
UC Merced Spring 2016 Magazine: **2016**
"All Go, No Quit: Student Demonstrates Her Drive"
Grossman Scholar in Chemistry & Chemical Biology at UC Merced **2015**
#Giving Tuesday School of Natural Sciences Scholar at UC Merced **2015**
Outstanding Student in Chemistry at Merced College **2013**

Teaching Experience:

General Chemistry Teaching Assistant **2018**
Biochemistry II Teaching Assistant **2018**
Instrumental Analysis Reader **2016**
Chemical Thermodynamics & Kinetics Reader **2016**
Tutor and Peer Mentor (Organic and Quantum Chemistry) **2015**

VI. Abstract

Title

Biophysical Analysis of Anti-Inflammatory Viral CC Chemokine Binding Protein vCCI

Laura Janelle Showalter

Master of Science

University of California, Merced

2018

Supervisor: Professor Patricia LiWang

Viruses have evolved mechanisms to subvert the immune system by interfering with chemokine signaling. The two mechanisms of evasion discussed in this thesis are proteins which bind chemokines to prevent them binding their receptors (as vCCI does) and chemokine analogs (such as vMIP-II) that competitively inhibit chemokines. Molecular dynamics simulations suggested that Y80 in vCCI is important for propping open the acidic loop, which keeps the binding site open. We investigated this hypothesis using ITC, NMR, and CD. For vCCI WT and vCCI Y80A, results included: a higher K_D for the mutant (2.99×10^{-8} M) when binding vMIP-II compared to vCCI WT ($\leq 1.00 \times 10^{-10}$ M), key residues involved in binding shifted in the unbound mutant NMR HSQC spectrum, and the mutant had lower stability demonstrated by a 6.1°C reduction in Tm. The Y80A mutation lowers chemokine affinity, which may indeed be due to collapse of the substrate-binding loop.

Chapter 1

Introduction

1.1 Chemokines and Inflammation

1.1.1 Inflammation

Inflammation occurs when there is an immune response in an area of the body. This commonly happens with injury or infection. The immune response is life-saving. It keeps foreign invaders out of the body and promotes the healing process. An important player in directing white blood cells to the area of interest are chemotactic cytokines, called chemokines. They are small proteins, about 8-10 kDa in size, which are secreted and mediate chemotaxis. The chemokines then create a chemoattractant gradient, with the greatest concentration of chemokines near the affected site and lessening with diffusion away from the site. Glycosaminoglycans (GAGs) promote their oligomerization and allow reversible immobilization, helping to form the gradient.[1] Circulating leukocytes have cell surface G-protein coupled chemokine receptors which will respond to extracellular chemokines and follow the chemokine gradient to the site of injury or infection.

While inflammation is an important part of the immune response, it also is involved in several pathologies. For instance, asthma is characterized by chronic swelling of the airway. Understanding inflammation and studying ways to perturb the immune response is key for the development of drugs for diseases that involve inflammation. Research in inflammation has wide applications in the medical field.

1.1.2 Chemokines and Chemokine Receptors

Humans have about 50 chemokines and 20 chemokine receptors.[2] Both the chemokines and the receptors that bind them are named in part by the conserved cysteine location patterns in the chemokines. There are 4 subclasses of chemokines: C, CC, CXC, and CX_3C, which indicates the proximity of cysteines to each other near the N-terminus of the chemokine (with X being an amino acid other than cysteine). An example of a chemokine name is CCL5: within the CC subclass, ligand 5. The receptor names have a similar naming convention, except they have R for receptor, instead of L for ligand (e.g. CCR5). The receptors are separated into these subclasses based on what subclass of chemokine they bind. Generally, receptors only bind one subclass of chemokines, but they can usually promiscuously bind several chemokines within that subclass.[1]

Chemokines have a characteristic Greek key fold with two disulfide bonds that include the cysteines near the N-terminus bonding to cysteines that are near the middle and end of the sequence. They have antiparallel β-sheets connected by loops, with an α-helix near the C-terminus.[1] The N-terminus is important for interaction with chemokine receptors, resulting in different levels of signaling and sequestration of the receptor.[3]

Chemokine receptors are G-protein-coupled receptors (GPCRs). GPCRs have seven transmembrane helices, with their N-terminus on the extracellular side of the membrane and their C-terminus on the cytoplasmic side. The N-terminus can become

post-translationally modified. Post-translationally sulfating tyrosine residues at the N-terminus of chemokine receptors to make them negatively charged has been shown to be important for tighter binding with positively charged chemokines.[4] Binding events can cause a structural change which allows G proteins, which are associated with the receptor on the cytoplasmic side, to become activated (replacement of GDP with GTP) and cause downstream signaling. The C-terminus is involved in receptor desensitization through becoming phosphorylated by βARK, subsequently associating with β-arrestin, and the receptor being endocytosed where it is dephosphorylated before returning to the cell surface.[1] There are additional ways the signal can be stopped besides desensitization. An effective signaling process must be able to stop after a stimulus has stopped and respond again when the stimulus reemerges.

1.1.3 Viral Subversion of the Chemokine Signaling Pathway

Several viruses have evolved means to subvert the immune system and allow for successful infection and reproduction using the host machinery. Some viruses dedicate half of their genome to evading the immune system.[5] Focusing on the chemokine signaling pathway specifically, it can be disrupted by stopping chemokines from binding to their receptors. This can be done in several ways, such as inhibition of chemokine production or maturation in the first place, blocking of the chemokine receptors' binding sites through chemokine analogs, and binding chemokines directly via chemokine binding proteins or receptor analogs so they cannot go on to bind their receptors, among other ways.[6] In my work, I have focused on the protein vCCI, encoded by poxviruses, which promiscuously and tightly binds the CC subclass of chemokines. I have also worked with vMIP-II, a protein encoded by herpesvirus that acts as a chemokine analog that binds chemokine receptors but generally does not cause downstream signaling. It competitively inhibits chemokine binding.

1.2 vMIP-II

1.2.1 Function

vMIP-II stands for viral macrophage inflammatory protein type II. It is a human herpesvirus-8 (HHV-8) encoded protein that is a chemokine analog. It binds and occludes chemokine receptors, generally without causing downstream signaling. Thus, it is chemokine receptor antagonist that operates as a competitive inhibitor. vMIP-II also binds GAGs more tightly than natural chemokines, further reducing inflammation by reducing the formation of a chemoattractant gradient.[7] Besides the anti-inflammatory properties of vMIP-II, it is also an HIV inhibitor due to its ability to bind both the co-receptors HIV exploits (CCR5 and CXCR4) to gain entrance into cells.[8]

1.2.2 Protein Characteristics

vMIP-II is 72 residues and about 8 kDa in size. It consists of a flexible N-terminus, followed by the N-loop, three β-sheets connected by loops, and an α-helix near its C-terminus.[8] It has a very similar structure to CC chemokines, with two disulfides located as expected for CC chemokines.

vMIP-II protein sequence used in experiments:
GLGASWHRPDKCCLGYQKRPLPQVLLSSWYPTSQLCSKPGVIFLTKRGRQVCADKSK
DWVKKLMQQLPVTAR

Table 1.1. vMIP-II Protein Characteristics

Characteristic	Value
Amino Acids	72
Molecular Weight	8186 Da
Theoretical pI	10.05
Extinction Coefficient	19730 $M^{-1}cm^{-1}$

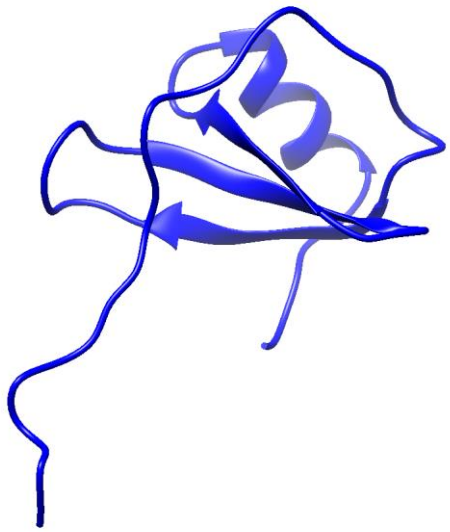

Figure 1.1. vMIP-II structure (PDB: 1VMP). Figure was made using UCSF Chimera.[9]

1.3 vCCI

1.3.1 Function

vCCI stands for viral CC chemokine inhibitor. As the name alludes, it promiscuously binds CC type chemokines, making them unable to bind to their endogenous receptors.[10–12] It is encoded by poxviruses. It binds many CC chemokines more tightly than their receptors do. Burns, et al. showed vCCI binding to over 80 viral, human, and murine CC chemokines, 26 of which were high-affinity binders (greater than 75% inhibition of MIP-1β binding to vCCI).[12]

1.3.2 Protein Characteristics

Historically, vCCI was called p35 for a protein having a mass of 35 kDa observed on SDS-PAGE.[11] The actual mass of the rabbitpox protein is about 26 kDa, but it runs a

little heavy (close to 35 kDa) on SDS-PAGE. While it binds chemokines tightly, its structure is not similar to chemokine receptors.[13] It is largely composed of β-sheets, with only one α-helix in the entire protein (which is more than 240 amino acids). It has 4 disulfide bonds and is very stable once folded.

vCCI 'wild-type' protein sequence (rabbitpox strain) used in experiments:
AMAASLQQSSSSSSSCTEEENKHHMGIDVIIKVTKQDQTPTNDKICQSVTEITESESDPD
PEVESEDDSTSVEDVDPPTT**Y**YSIIGGGLRMNFGFTKCPQIKSISESADGNTVNARLSS
VSPGQGKDSPAITHEEALAMIKDCEVSIDIRCSEEEKDSDIKTHPVLGSNISHKKVSYEDII
GSTIVDTKCVKNLEFSVRIGDMCKESSELEVKDGFKYVDGSASKGATDDTSLIDSTKLK
ACV

Note: the first 3 amino acids (colored purple) in the sequence are slightly modified to allow for a NcoI cut site at the beginning of the gene. The true wild-type sequence is MP- instead of AMA-. I will refer to this sequence as WT throughout my thesis. The 80th residue, which is a tyrosine, is bolded and underlined.

Table 1.2. vCCI Protein Characteristics for wild-type and each vCCI mutant used in experiments.

Characteristic	WT	Y80A	13 aa N-term trunc
Amino Acids	243	243	230
Molecular Weight	26174 Da	26082 Da	24938 Da
Theoretical pI	4.51	4.51	4.51
Extinction Coefficient	6460 $M^{-1}cm^{-1}$	4970 $M^{-1}cm^{-1}$	6460 $M^{-1}cm^{-1}$

Figure 1.2. vCCI structure (PDB: 2FFK). Figure was made in UCSF Chimera.[9]

1.3.3 Therapeutic Potential

The therapeutic potential of vCCI has been well noted in the literature. Its promiscuous binding of chemokines lends itself to use as a drug to potentially treat various conditions that are characterized by excessive and chronic inflammation, such as traumatic brain injury, asthma, and arthritis. Alcamí, et al. illustrated the ability of vCCI to block eotaxin-induced eosinophil infiltration in guinea pig skin by checking eosinophil accumulation 2 hours after various mixtures of eotaxin and vCCI were intradermally injected in guinea pigs.[13] Buatois, et al. showed the efficacy of vaccinia virus (Lister strain) vCCI attached to a human IgG1 Fc domain in mice by stopping cell migration to locally inflamed tissue in an air pouch model and by interfering with collagen-induced arthritis.[14] White, et al. showed vaccinia virus (Lister strain) vCCI attached to a human IgG1 Fc domain inhibited CC chemokine-induced calcium flux, chemotaxis, and β-arrestin recruitment in murine primary macrophages and transfected cells.[14] Dabbagh, et al. demonstrated the ability of cowpox vCCI to treat asthma in mice when administered intranasally. They found that vCCI greatly reduced inflammation in the airway and the lung parenchyma, while it did not change immune responses systemically (at extrapulmonary sites).[15]

1.3.4 Relevant Mutations in Literature

In the same paper referenced above, White et al. made mutations to vCCI (which was attached to a human IgG1 Fc domain) based on previously published structural data[15] by Zhang, et al. to see how that would change its ability to reduce chemokine signaling. The mutations Y80A, R89A, D141A, D141L, D141R, E143A, E143K, E143R, V185A, Y217A, and Y217N were all made and tested.[16] 15 nM vCCI (WT or mutants) was pre-incubated with 5 nM RANTES for 2 hours before being added to cell culture. WT vCCI-Fc produced only 38% of the response of RANTES by itself. They expected and found the charge swap mutants of 143 to have a complete (>95%) loss of function. Mutations to 141 reduced vCCI's function. The mutations made to 217 worsened vCCI's function. V185A somewhat improved the function of vCCI. They expected both R89A and Y80A to improve the ability for vCCI to block chemokine signaling.[16] They thought that removing the relatively bulky Y (80th residue) and R (89th residue) from the binding pocket would improve binding. R89A did indeed enhance vCCI's function. However, Y80A showed complete loss of function. They rationalize that Y80A must make a critical contact for binding with K48 in RANTES.[16]

Arnold, et al. studied the following mutants of mousepox vCCI (referred to as EVM1 in the paper): Y69R, S134R, N136W, S171W, S171Y, I173Y, I173R, and Δ51-65.[17] Using SPR (Surface Plasmon Resonance) with human MIP-1α, they found L125R improved binding by 1.7x and E17R & K138Y had only a slightly smaller K_D than WT. All the other mutants worsened binding, especially I173R and Δ51-65. They expected the Y69R mutant to be a worse binder because it places R near a positively charged residue in the chemokine.[17] Y69R, comparable to Y80 in rabbitpox, reduced binding affinity by 52x, giving an apparent K_D of 1.50 nM $\pm$ 0.30 nM compared to 0.029 nM $\pm$ 0.011 nM for WT. It is noted that the on rate was not affected by this mutation.

1.4 Summary

1.4.1 Summary of vCCI:vMIP-II Complex

The complex between vCCI and vMIP-II was investigated by our group because they both evolved to be complimentary to each other. vCCI evolved to tightly bind chemokines, while vMIP-II evolved as a chemokine analog. vCCI binds vMIP-II with a very high affinity, shown to be 0.06 nM $\pm$ 0.006 nM through competitive fluorescence experiments in our lab by Nai-Wei Kuo.[18] This complex takes two viral proteins evolved to promiscuously bind their targets, chemokines for vCCI and chemokine receptors for vMIP-II, and shows how well they both do what they have evolved to do. Previously, our group carried out NMR experiments to determine which regions of the proteins are important for binding, as evidenced by chemical shift change upon complex formation.[18] vCCI experiences the largest chemical shifts upon vMIP-II binding in the residues in the 80's, 140's, and 190's, with other notable shifts in the 30's, 170's, 180's, and 220's regions. Many of these regions are in β-sheets in vCCI's binding pocket. The acidic loop in the 50's to 70's region that is shown to be involved with binding by molecular dynamics simulations are hard to see by NMR due to their flexibility.[18] Negatively charged residues D141 and E143 are important for binding. For vMIP-II, NMR chemical shift changes upon vCCI binding are the largest for its N-loop region and two of its β-sheets, corresponding to residues in the 10's, 30's and 50's regions.

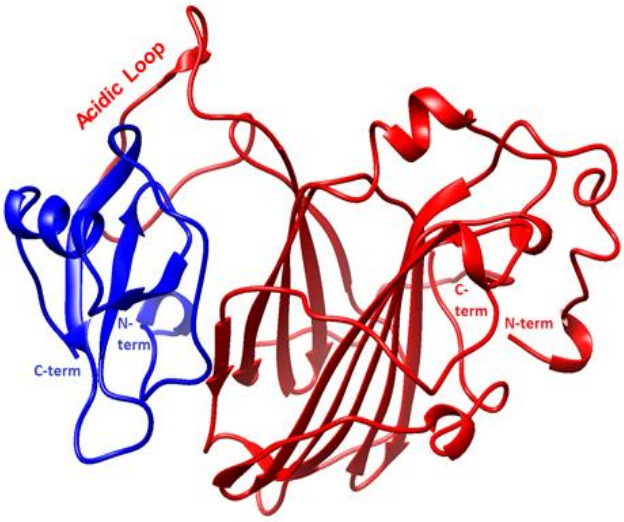

Figure 1.3. The vCCI:vMIP-II complex after 1 microsecond of MD simulation, performed by Michael Colvin. Presented in Figure 4A of our previously published paper.[18] vMIP-II is shown in blue and vCCI is shown in red. The figure was made in UCSF Chimera.[9]

1.4.2 Hypothesis and Techniques Used

For this master's degree work, we decided to explore the interesting effect of the Y80A mutation in vCCI. Our group's previous structural results indicated the vCCI Y80 was located at the base of the acidic loop, near the binding site of chemokine ligands.[10] The tyrosine at that location could possibly be sterically impeding the chemokine's

arginine near that location in the binding pocket. The results of Arnold, et al. supported this idea through their Y69R mutation in mousepox leading to lower affinity of the vCCI:chemokine complex.[10] Their mutant both maximized steric and charge repulsion at that site. Additionally, Beck, et al. showed that MCP-1 K49A (a chemokine residue close to the 80th position of vCCI when bound) increased affinity to vCCI by 3x.[19] This all led to White, et al. mutating the tyrosine at the 80th position to alanine, hypothesizing that this would increase vCCI binding affinity through lowering steric repulsion with the chemokine.[16] However, they found the opposite: the Y80A mutation caused vCCI to lose function. They did not have a solid reason for why this was the outcome, which intrigued our collaborator, Dr. Michael Colvin. Through analysis of his molecular dynamics (MD) simulation data, he came up with the hypothesis that Y80 could be holding the acidic loop open, exposing the binding site of vCCI. Mutating the bulky Y80 to a smaller alanine could destabilize the loop position. His and his graduate student Lauren Stark's simulation data on this indicates that the Y80A mutation causes the loop to collapse onto the β-sheets of the binding site. Their simulation results are shown in Figures 1.4 to 1.6. Figure 1.4 shows vCCI WT after 1 microsecond of simulation time, with the loop open. Figure 1.5 shows vCCI Y80A after both 1 microsecond and 2 microseconds of simulation time. At 1 μs, the loop is partially collapsed, having some interactions with the β-sheet below, especially R149. At 2 μs (and prior), the loop is fully collapsed onto the β-sheets below and P58 on the loop is in a pocket formed by the β-sheets.

Figure 1.4. vCCI WT after 1 microsecond of simulation time, performed by Lauren Stark. Y80 is colored in yellow, with its side chain showing. The figure was made in UCSF Chimera.[9]

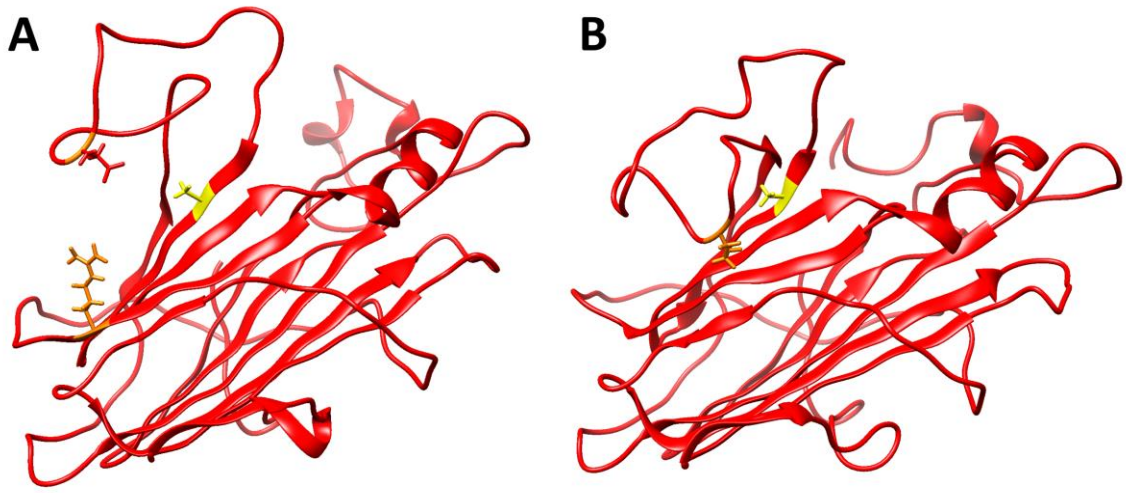

Figure 1.5. vCCI Y80A after (A) 1 microsecond of simulation time and (B) 2 microseconds of simulation time, performed by Lauren Stark. At 1 microsecond, the acidic loop is partially collapsed. It fully collapses and stays stably down up to 2 microseconds (this is the longest simulation to date). The 80th residue alanine is in yellow with its side chain showing in both (A) and (B). Interacting residues are shown in orange with their side chains showing in both (A) and (B). In (A), E63 on the loop is shown near R149 on the β-sheet below. In (B), P58 on the loop is in a pocket in the β-sheets. The figure was made in UCSF Chimera.[9]

During their vCCI Y80A simulations, they have seen the floppy N-terminus interact with the acidic loop when it collapses, in some cases assisting to keep it open. This is shown in Figure 1.6, below. D73 and D75 are seen in close proximity to the positively charged N-terminus. We were interested in whether the N-terminal tail contributes to keeping the loop open. For these reasons, we decided to make both the Y80A mutant and a 13 amino acid (12 amino acids if considering the true WT sequence, see section 1.3.2 for further explanation) N-terminal truncation mutant to test experimentally.

Figure 1.6. vCCI Y80A after 500 nanoseconds (0.5 microseconds) of simulation time, performed by Lauren Stark. The 80th residue alanine is in yellow with its side chain showing. D73 and D75 (colored orange) and seen interacting with the positively charged N-terminus (colored green). The figure was made in UCSF Chimera.[9]

I made the Y80A and 13 aa N-terminal truncation mutants and expressed them in *E. coli*. I optimized purification protocols. Then I used CD, NMR, and ITC to test them (except the truncation mutant has not yet been tested). The proteins' secondary structure and stability were tested by doing a temperature ramp of vCCI WT and vCCI Y80A. NMR HSQC spectra were obtained for both vCCI WT and vCCI Y80A, and changes in chemical shift were analyzed to see changes in the chemical environment of various residues. ITC was used to perform binding experiments of vCCI WT and vCCI Y80A with vMIP-II to determine if there was a change in K_D with the mutant.

Chapter 2

Creation of Mutants and Protein Expression & Purification

2.1 vCCI Mutations

As discussed earlier, the two mutants of vCCI produced were vCCI Y80A and 13 aa N-terminal truncation vCCI (referred to as 13 aa Nt-trunc vCCI from here on out). Two-step PCR was used to create both mutants. While usually one-step PCR would be fine for an N-terminal truncation mutation in DNA, it was more complicated in this case due to the 7 poly-serine protein sequence in the desired truncation region (see Section 1.3.2 for the vCCI protein sequence). It is difficult to not get slippage of the primer needed for that region in a one-step PCR. For point mutations, two-step PCR or Quikchange® can be used. Two-step PCR was chosen as the strategy for both mutations and they were both successful. Below, the primers and strategies used for the Y80A mutation are shown in Table 2.3 and Figure 2.2, respectively, and for the 13 aa Nt-trunc mutation, they are shown in Table 2.4 and Figure 2.3, respectively. Below, the troubleshooting and optimization that led to the optimal conditions for each mutation are discussed.

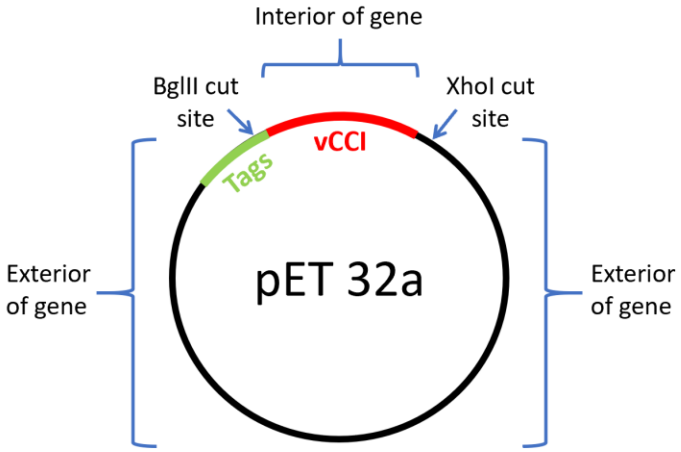

Figure 2.1. Vector layout for vCCI gene inside of the pET 32a vector.

First, the possible regions that could be selected in the vector and gene had to be analyzed when designing the primers. See Figure 2.1 for the layout of the vector used and for reference when discussing primer design. The primers on the exterior of the gene (1 and 4 in the below tables and figures) were easier and could wait to be decided on until the end because there was a large amount of length from which to choose. Thus, the mutational primers (the primers that will actually be causing the mutation on the interior of the gene), which could not easily be changed, were the primary focus. Once the mutational primers are designed, it is simple to find good candidates for the exterior of the gene. To save some money and hassle, primers #1 and 4 were designed to be the same for both mutations because vCCI was in pET 32a, so the sequences around the gene remained the same. Restriction enzyme cut sites available around the gene were checked using the NEBcutter V2.0 tool. It is ideal that

two different enzymes are used and that there is only one cut site for each. To check if there was a compatible buffer for a given set on enzymes, the NEB RE Digest tool was utilized. Once the cut sites are known, the exterior primers must be far enough away from the gene that the desired cut sites are included in the PCR products. This allows for the PCR product to be cut and ligated back into the vector.

Primer lengths of about 20 bp were aimed for, with a C or G on the ends of the oligo to help it better bind to the template DNA. Then, the oligo's melting temperature (Tm) was checked using the NEB Tm Calculator with Phusion High-Fidelity DNA Polymerase (HF Buffer) selected. The desired result for the melting temperatures was for them to be between 55°C and 65°C and for all the primers to be within about 5°C of each other. Then, the IDT DNA Analyzer tool was utilized to check that the most favorable hairpin Tm was below the primer's melting temperature by 15°C or more. Also, it could cause problems if self- or hetero-dimerization of the oligos are too favorable. All the combinations of primers in the reactions needed to be checked in IDT's tool.

For each PCR, gradient PCRs were done to test a variety of annealing temperatures. First, for the 1st step PCRs, 4 separate reactions were done with annealing temperatures from approximately 58°C to 66°C, at increments of 2°C, using the DNA polymerase Taq pol at first to scout inexpensively. The following program was used on the Eppendorf Mastercycler® Gradient thermocycler:

Table 2.1: Initial method for Taq pol scouting 1st step PCR reactions. Tubes were placed in columns 1 (58.1°C), 4 (60.7°C), 5 (62.5°C), 6 (64.6°C) and 7 (66.7°C).

Step	Temp (°C)	Duration (min:sec)	Step Explanation	
1	95	1:00	Initial denaturation	
2	95	1:00	Denaturation	Steps 2-4 Repeat 28x
3	66 (G=7.8)	1:00	Annealing	
4	72	1:00	Elongation	
5	72	2:00	Elongation to finish any left-over fragments	

Sizes were checked under UV light after reactions were run on 1.2% agarose gels containing EtBr at 100 V for 40 minutes. All reactions worked except the truncation reaction results for the 1st Step PCR (a) (see Fig 2.2) couldn't be visualized on the gel. For the Y80A reactions, 58°C worked best as the annealing temperature. Whereas, for the truncation reaction that could be seen on the gel, 62.5°C worked best. Phusion pol (higher quality DNA polymerase) was used going forward because there was a good idea of what annealing temperatures would work. With Phusion, the following method was used:

Table 2.2 Phusion method for 1st step PCR reactions. Tubes were placed in columns 1 (58.1°C) for Y80A reactions and 5 (62.5°C) for truncation reactions.

Step	Temp (°C)	Duration (min:sec)	Step Explanation	
1	98	0:30	Initial denaturation	
2	98	0:10	Denaturation	Steps 2-4 Repeat 30x
3	66 (G=7.8)	0:45	Annealing	
4	72	1:00	Elongation	
5	72	10:00	Elongation to finish any left-over fragments	

All the reactions were the expected size. The reaction tubes were PCR purified. Then, 35 ng of DNA from each of the two 1st step reactions for each mutant were combined. The first part of the 2nd step PCR was elongation of the PCR products, which overlap each other (see figures 2.1 and 2.2). This was done by repeating the Phusion method above, but with no primers present, an annealing temperature of 62°C with no gradient, and only repeating Steps 2-4 10x. After that finished, primers were added and the Phusion method was done again (still with an annealing temperature of 62°C), but this time repeating Steps 2-4 30x, like normal. The truncation mutant was confirmed to be the right size, but the Y80A mutant was not. This was troubleshooted by repeating the 2nd step PCR with an annealing temperature gradient, trying 52°C, 54.2°C, 56°C, 58.1°C, 60.2°C, 64.5°C (having already tried 62°C). The annealing temperature that worked was 56°C, with none of the other temperatures resulting in the correct size of PCR product.

Table 2.3. vCCI Y80A primers (numbers correspond to Figure 2.2). Tm is based on NEB Tm Calculator with Phusion High-Fidelity DNA Polymerase (HF Buffer) selected.

vCCI Y80A			
Primer	Sequence (5’ — 3’)	Length (bp)	Tm (°C)
1	CTG TTC AAA AAC GGT GAA GTG	21	62
2	GAT GAT GGA GTA AGC AGT GGT AG	20	62
3	CTA CCA CTG CTT ACT CCA TCA TC	20	62
4	GAT CTC AGT GGT GGT GGT G	19	62

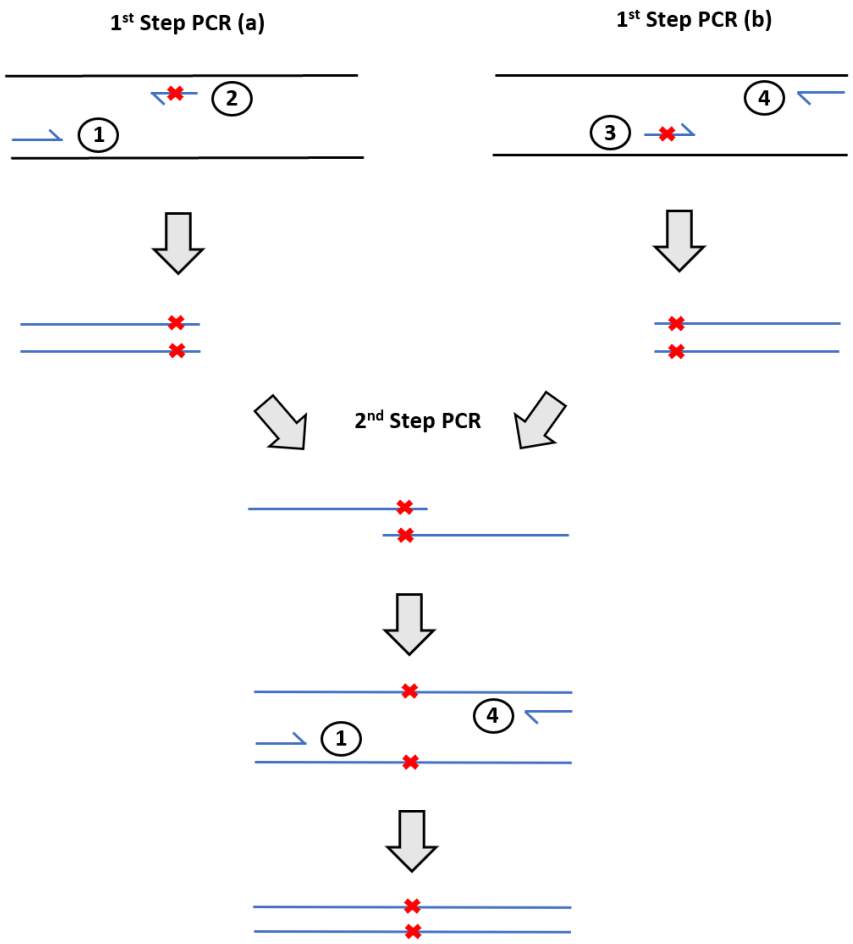

Figure 2.2. vCCI Y80A mutation strategy. The numbered primers are listed in Table 2.3. The red X's correspond with the Y80A mutation introduced into the DNA through the mutational primers. The arrows at the ends of the primers indicate direction of polymerization—they are not overhangs. The DNA segment shown above is a zoom in on the Tags and vCCI gene region of the vector. The cut sites that will be used later on are within the PCR product.

Table 2.4. N-term 13 aa truncation vCCI primers (numbers correspond to Figure 2.3). Tm is based on NEB Tm Calculator with Phusion High-Fidelity DNA Polymerase (HF Buffer) selected.

N-term 13 aa truncation vCCI			
Primer	Sequence (5' — 3')	Length (bp)	Tm (°C)
1	CTG TTC AAA AAC GGT GAA GTG	21	62
2	GAG GAC TTG TCG TCG TCG TC	20	65
3	GAC AAG TCC TCA TCC TCG TGT AC	23	64
4	GAT CTC AGT GGT GGT GGT G	19	62

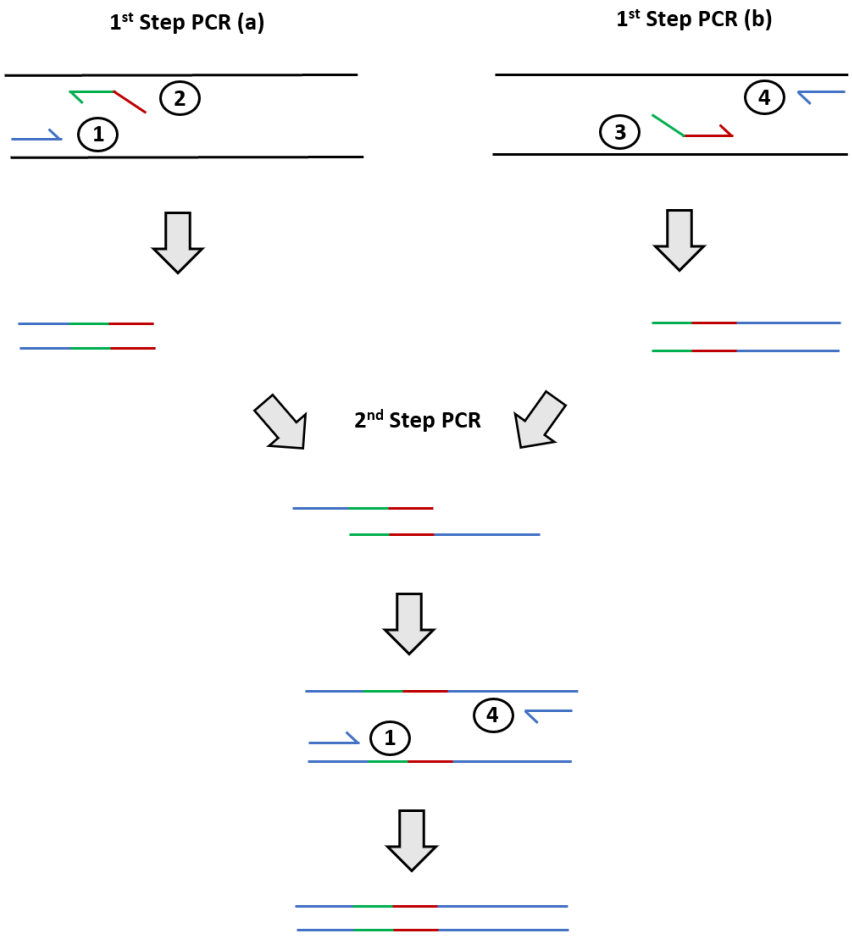

Figure 2.3. vCCI 13 aa N-term truncation mutation strategy. The numbered primers are listed in Table 2.4. The green and red portions are the areas that were on either side of the area that was truncated. The arrows at the ends of the primers indicate direction of polymerization—they are not overhangs. The primers that have a longer red or green overhang (as in primer #2 and #3) without an arrow on that end are actual overhangs. The DNA segment shown above is a zoom in on the Tags and vCCI gene region of the vector. The cut sites that will be used later on are within the PCR product.

The PCR products and pET 32a vector were all double digested with BglII and XhoI in NEB Buffer 3.1 (the only buffer with 100% activity for both restriction enzymes on NEB Double Digest Finder) at 37°C. SAP was added to the cut pET 32a vector at the end of the digest reaction to avoid vector reclose using ligation. The cut bands were gel extracted and purified. The cut mutant PCR products were combined with the cut vector (in a 9:1 ratio based on their concentration, adjusted for their size: $^{ng}/_{(\mu L * bp)}$) and were ligated together by T4 ligase for 1 hour at room temperature. The resulting ligated 2nd step PCR products in pET 32a were transformed into XL1 Blue cells, plated and incubated at 37°C, then single colonies were chosen to grow up by shaking in LB with antibiotic they have resistance to for 16 hours at 37°C, then miniprepped. The resulting

minipreps were sequenced at the UC Berkeley DNA Sequencing Facility with either T7 promotor or reverse primers. They were successful. The final PCR conditions that worked are listed in Table 2.5.

Table 2.5. Optimized annealing conditions for Y80A and truncation mutants' PCRs.

PCR Step	Y80A (°C)	13 aa Nt-trunc (°C)
1 (a)	58	62.5
1(b)	58	62.5
2	56	62
2 (after primer addition)	62	62

2.2 Protein Expression

vCCI WT and mutants were contained in the pET 32a expression vector, which has ampicillin resistance. vMIP was contained in a pET 28a expression vector, which has kanamycin resistance. A fresh transformation was done with *Escherichia coli* BL21 (DE3) (Novagen) competent cells, then plated onto 100 µg/mL ampicillin or 50 µg/mL kanamycin agar plates and incubated at 37°C for 12 hours. Starter cultures were made with 7 mL LB with either 100 µg/mL ampicillin or 50 µg/mL kanamycin, and 15 colonies from the corresponding antibiotic plate. These were shaken at 37°C for 2 hours before being put in 1 L of either warmed LB (^{14}N) or M9 minimal media (with the sole nitrogen source being $^{15}NH_4Cl$), with the same antibiotic concentration as the starter cultures. The media was shaken at 37°C until the OD_{600} of the cells was approximately 0.7. At that point, 0.7 mM IPTG final concentration was added to induce the cells. They expressed for 20 hours at 22°C while shaking. Afterward, the media was centrifuged at 4400 x g for 10 minutes at 4°C. The supernatant was decanted, then the pellet was resuspended in 6 M Guanidine HCl, 200 mM NaCl, 50 mM Tris, pH 8.0.

2.3 Protein Purification

In all cases, the resuspended pellets with approximately 10 mM benzamidine (a protease inhibitor) were passed through a French Press three times to lyse the cells before being centrifuged at 27000 x g for 1 hour at 4°C. The supernatant (which contained the protein of interest due to its being soluble in the guanidine buffer) was decanted into polypropylene tubes and allowed to sit at -20°C overnight to allow for further separation of cell debris. The tubes were spun down for an additional 15 minutes at about 3400 x g at 4°C to further pellet cell debris. See each subsection below to see the rest of the purification protocol for vCCI (WT and mutants) and vMIP-II. SDS-PAGE was used throughout the expression and purification process to monitor the protein size. NMR HSQCs for ^{15}N-labeled samples or echo11 for ^{14}N samples were obtained at the end of the purification process to confirm proper folding.

2.3.1 vCCI WT and Mutants

This protocol is an adaptation of the protocol used in our previous paper.[18] The protein construct has both a thioredoxin (Txn) tag and a 6x-His tag at its N-terminus with a DDDDK cut site in between the tags and the protein of interest (vCCI), so the tags can later be cleaved off by enterokinase (EK). The His tag is in the middle of the Txn tag and vCCI, so to help expose the His tag, the supernatant was reduced with 15 mM βME for two hours at room temperature before passing through a home-packed gravity nickel column. The nickel column was equilibrated in the same lysis buffer and 15 mM βME. Subsequently, the protein supernatant was passed through the column 2x. Then, the column was washed with 10 column volumes of 6 M Gnd-HCl, 200 mM NaCl, 50 mM Tris, pH 8.0, 15 mM βME, followed by 10 column volumes of 6 M Gnd-HCl, 200 mM NaCl, 80 mM NaOP, pH 7.0, 15 mM βME. The protein stuck to the column was then eluted off with 6 M Gnd-HCl, 200 mM NaCl, 60 mM NaOAc, pH 4.0. The fractions identified by absorbance at 280 nm to have the majority of eluted protein were collected in a polypropylene tube, then βME was added to bring its concentration to 25 mM. A small stir bar was put in the tube, then stirred at room temperature for one hour before stirring at least 12 hours at 4°C. This step was needed to ensure all disulfides were reduced in the protein (one disulfide in Txn and four in vCCI).

The protein was drip refolded into 20x volume refold buffer (550 mM L-Arg HCl, 400 mM sucrose, 9.6 mM NaCl, 0.4 mM KCl, 2 mM $CaCl_2$, 2 mM $MgCl_2$, 3 mM GSH, 0.3 mM GSSG, 50 mM Tris, pH 8) that was cooled by ice and within a 4°C fridge beforehand. The protein was allowed to refold for at least 24 hours at 4°C while stirring. Note that long reduction and refold times, low temperatures, and greater than normal concentration of redox pair (glutathione) proved to be essential for proper refolding of the protein. After refolding, the solution was put into 10 kDa MWCO dialysis bags and dialyzed into 4 L of 20 mM Tris, 2 mM $CaCl_2$, 200 mM NaCl, pH 7.4 three times at 4°C. On the third dialysis, EK was added to the bags for 20 hours to cleave the tags off. Cutting is visible by SDS-PAGE, with vCCI running at about 35 kDa and the tags running at about 17 kDa.

After cutting, the protein was dialyzed into the buffer used for SEC: 20 mM Tris, 200 mM NaCl, pH 7.4 (very similar to the cutting buffer, just without the $CaCl_2$). The protein was then concentrated about 55x because it was dilute to allow for better refolding, but SEC resolution depends on loading only a small volume onto the column. Each run was done by loading 5 mL of concentrated protein onto a HiLoad® 16/600 Superdex® 75 prep grade (GE Healthcare) SEC column on the AKTA system. This column has a column volume of 120 mL. Large molecules come through an SEC column first because they have a shorter average path length through the column. Smaller molecules have a larger path length because they enter pores in the resin while traveling down the column. All runs were performed by equilibrating the column with 96 mL of SEC buffer at a 0.8 mL/min flow rate and 0.5 MPa pressure alarm. vCCI comes out at about 70 mL after injection. The protein is stable to store at 4°C for long periods of time. vCCI was concentrated in an Amicon concentrator with a 10 kDa filter prior to ITC experiments.

2.3.2 vMIP-II

This protocol is an adaptation from the protocol used in our previous paper.[18] This protein made from the pET 28a construct has both a SUMO tag and a 6x His tag at its N-terminus which are cleaved off by ULP-1 later in the purification process. ULP-1 cleaves conditional upon SUMO having a properly folded tertiary structure. Home-packed gravity nickel columns were equilibrated in the same buffer used when lysing the cells. The protein supernatant was passed through the column 2x. Then, the column was washed with 10 column volumes of 6 M Gnd-HCl, 200 mM NaCl, 50 mM Tris, pH 8.0, followed by 10 column volumes of 6 M Gnd-HCl, 200 mM NaCl, 80 mM NaOP, pH 7.0. The protein stuck to the column was then eluted off with 6 M Gnd-HCl, 200 mM NaCl, 60 mM NaOAc, pH 4.0. The fractions identified by absorbance at 280 nm to have the majority of eluted protein were collected in a polypropylene tube, then βME was added to bring its concentration to 10 mM. A small stir bar was put in the tube, then stirred at room temperature for 2 hours before drip refolding. The reduction and refolding protocol for vMIP is less extensive than for vCCI because vMIP only has 2 disulfide bonds and SUMO has zero disulfide bonds (no free cysteines either). The protein was dripped into 10x refold buffer: 550 mM L-Arg HCl, 200 mM NaCl, 1 mM EDTA, 1 mM GSH, 0.1 mM GSSG, 50 mM Tris, pH 8. After dripping was complete, the solution was put into the 4°C fridge to refold for at least 12 hours.

After refolding, the solution was put into 3.5 kDa MWCO dialysis bags and dialyzed into 4 L of 20 mM Tris, 200 mM NaCl, pH 8.0 three times at 4°C. On the third dialysis, ULP-1 was added to the bags at least 12 hours to cleave the tags off. Cutting is visible by SDS-PAGE, with vMIP-II running just above 6.5 kDa and the tags running at about 18 kDa. To separate cut vMIP-II from the tags, a 5 mL HiTrap Heparin HP affinity column (GE Healthcare) was used on the AKTA system. This was very effective and seemed to work better (with higher yields) than a native nickel column. It is necessary to remove the tags before using a C4 column because the tags and vMIP-II elute off the C4 column at the same acetonitrile concentration. The protein was dialyzed into 4 L of 50 mM Tris pH 7.4. The Heparin column was equilibrated with 10 column volumes of 50 mM Tris pH 7.4 buffer before the dilute protein was added to the column via a 110 mL external loop at a rate of 5 mL/min with an alarm pressure of 0.5 MPa. Once all the protein was loaded, the Tris concentration and pH stayed constant while there was a gradient from 0 to 1 M NaCl. Salt knocks protein off in the order of least affinity to most affinity for heparin. vMIP-II comes off the column at around 50% B (500 mM NaCl), while the tags come off near the beginning of the gradient (at low salt concentration), separating them very well.

For the benefit of removing salt and getting the protein in the stable form of lyophilized powder, a C4 (Vydac) column with a 20 mL column volume was used on the AKTA system as the final purification step. The post-Heparin fractions needed to be dialyzed into lower salt (<100 mM NaCl) before running on the C4. One dialysis into 4 L 20 mM Tris, 80 mM NaCl, pH 8.0 was sufficient. The protein was then prepared for loading by centrifuging the sample at 3400 x g for 10 minutes at 4°C. Afterward, 0.2% TFA was added to the sample, checked by pH paper to be around pH 1-2, then 10% Acn (stock containing 0.1% TFA also) was added. The C4 column was equilibrated with 4 column volumes of 10% Buffer B (10% Acn/90% H_2O, 0.1% TFA) at a rate of 5 mL/min. Buffer A is H_2O, 0.1% TFA and Buffer B is Acn, 0.1% TFA. The acid is necessary for the proteins loaded not to stick too hard to the column, giving them the ability to be eluted by

increasing the concentration of acetonitrile. The samples were loaded onto the column through an external loop by pushing 1.5x the volume of protein in the loop through it with 10% B. The first gradient in the program is from 10% B to 28% B at 5 mL/min, then the rate is dropped to 2 mL/min while going on a gradient from 28% to 36% B over 4 column volumes. The sample should already be very pure at this point and should come off at about 34% B. The post-C4 fractions can be lyophilized on a Labconco freeze-dry system and then stored at room temperature, away from light. When preparing for various experiments, the powder should be taken up in 20 mM NaPi (or similar) pH 2.5. It will dissolve really easily and then can be diluted into other buffers as needed. Aggregation is a real problem in higher pH buffers, so always take up the powder in pH 2.5 buffer first. See more discussion about this in Section 3.3.1 (ITC Theory and Method).

2.4 Discussion & Future Directions

These methods can be further improved by testing more expression conditions, IPTG concentrations, and different expression systems. Notably, vMIP-II has some small degradation post-ULP-1 cutting (shows up just below 6.5 kDa on SDS-PAGE) which can be separated by the Heparin column, but it does lower the overall yield. A different tag/expression system may help prevent this issue. Also, moving through the purification process as quickly as possible lowers degradation as well. Anna Nguyen, Ph.D. graduate from the P. LiWang Group in 2017, noted that expression in the pET 32a expression vector and subsequent cutting with EK chopped the protein up much worse.

More vCCI mutants are needed to further test our hypotheses. Some of these additional mutants are already made in DNA with the help of Kathryn Fischer, a current Ph.D. student in the P. LiWang Group at UC Merced. The additional mutants focus on adding a Q to the N-terminus in order to later cyclize the Q and thus eliminate the positive charge of the N-terminus. Double and triple mutants with Y80A, truncations, and Q0 are also of interest going forward with this project. I suspect that the purification protocol I describe above will continue to work for these new mutants of vCCI.

Chapter 3

Theoretical Background of Techniques & Results

3.1 Circular Dichroism

3.1.1 Theory and Method

Circular dichroism (CD) measures the difference in absorbance of left- and right-polarized UV light. Thus, to have a signal, the molecule must absorb them differently, indicating the molecule must be chiral or at least in a structured environment. CD can be used to detect tertiary structure via aromatic side chains in the near UV range (250 – 350 nm), or much more commonly, secondary structure via backbone amide bonds in the far-UV range (170 – 250 nm).[20] β-sheets have a characteristic minimum at approximately 215 nm.[21] Whereas, α-helices have two minima at about 210 and 220 nm. A random coil has an entirely different profile, with a minimum around 195 nm and a maximum near 210 nm. Both β-sheets and α-helices have maxima around 190 nm, in contrast. However, it is difficult to see in that range because it tends to get noisy from buffer components that absorb near that area. The noise level depends on what buffer conditions are used; low salt is optimal.

The experimental results shown in Section 3.1.2 were obtained on a Jasco J-1500 Circular Dichroism Spectrophotometer. A 25°C to 95°C temperature ramp was performed on 15 μM samples of vCCI WT and vCCI Y80A in 20 mM NaPi, 100 mM NaCl, pH 7.0. The temperature gradient was 1°C/min, with 215 nm monitored continuously (data collected every 0.2°C). A full spectrum (260 – 190 nm) measurement was taken every 10°C. All graphs presented in Section 3.1.2 were generated using the Origin software package. The data was normalized based on the CD ratio between the vCCI WT and vCCI Y80A at the isodichroic point for both of them at 209 nm (where all the curves from various temperatures intersect). Thus, the magnitude at 209 nm is based upon the concentration of the sample, not the fold of the protein. The ratio was 0.93, small enough that it can be attributed to absorbance error and/or other errors in transferring volumes for the dilutions. Thanks to Prof. Shahar Sukenik for assistance in processing the data shown below.

3.1.2 Results and Discussion

In Figure 3.1, the far-UV CD spectrum of vCCI WT and vCCI Y80A are overlaid at the beginning and end of the temperature ramp from 25°C to 95°C. The spectrum of each before and after the temperature ramp is near identical, suggesting similar folded and unfolded states. At 25°C, they both have a minimum at about 215 nm (marked by the grey vertical line), the characteristic minimum corresponding to β-sheets. The 95°C spectra look like what would be expected for unfolding.[22] The minimum is no longer at 215 nm and is shifted to lower wavelengths. There is noise near the 190 nm area, so the true minimum may be masked by the buffer noise.

Figure 3.2 shows the signal at 215 nm for both vCCI WT and vCCI Y80A throughout the temperature ramp. The less negative the θ at 215 nm, the less β-sheet structure present in the sample. As the temperature increases, so does the ellipticity at a

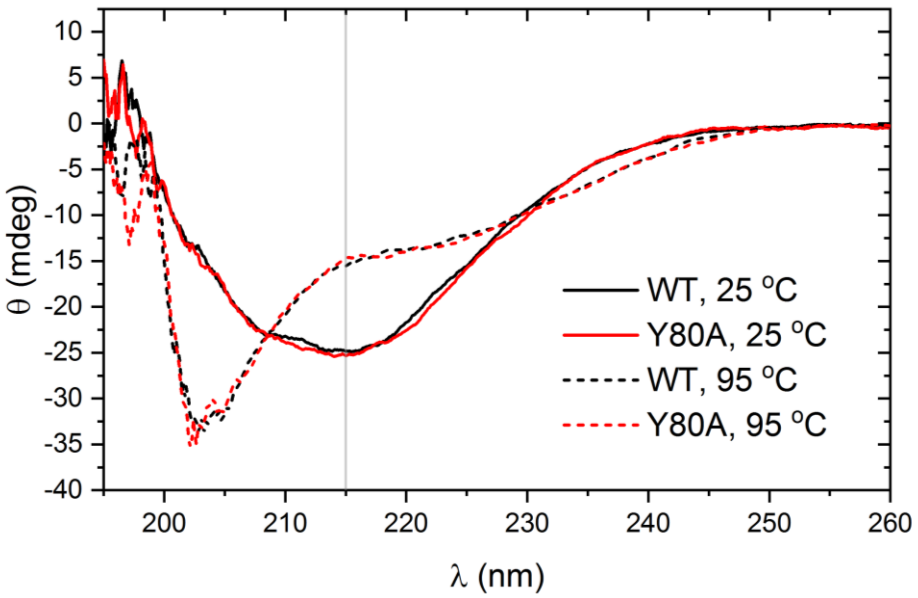

Figure 3.1. Far-UV CD spectrum of vCCI WT (in black) and vCCI Y80A (in red) overlaid at the beginning and end of a temperature ramp from 25°C to 95°C. The grey vertical line on the graph is at 215 nm (characteristic minimum corresponding to β-sheets).

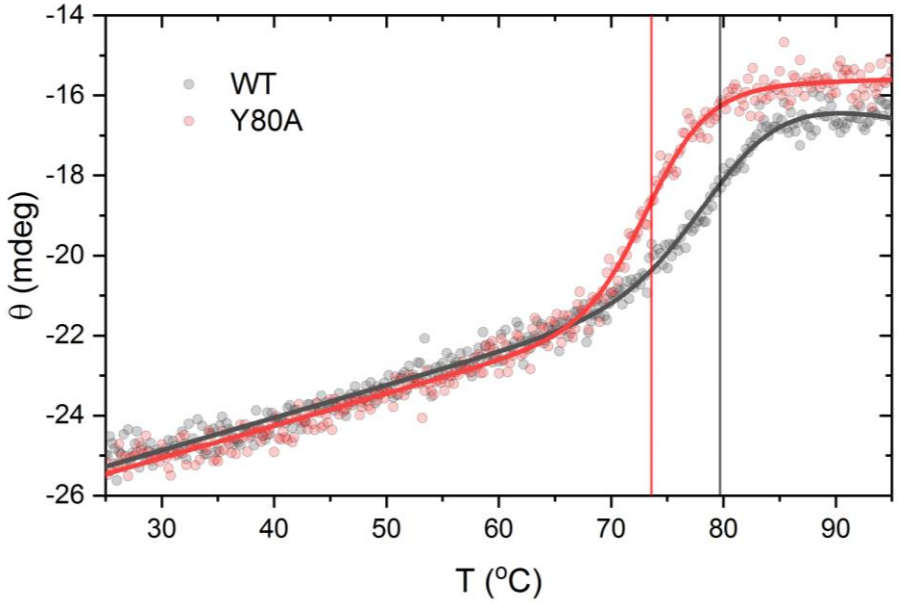

Figure 3.2. Ellipticity at 215 nm of vCCI WT and vCCI Y80A over the course of a temperature ramp from 25°C to 95°C. Note the scale is changed from Figure 3.1. The black and red vertical lines on the graph are at the melting temperature values of vCCI WT and vCCI Y80A, respectively. Data points are shown, with trendlines presented as solid lines. The adjusted R^2 is 0.99178 and 0.99360 for the vCCI WT and vCCI Y80A fitted line, respectively.

constant slope, until near 70°C, a more rapid (larger slope) transition begins. The temperature at which there is an inflection point of the curve (where the second derivative is equal to 0) is the melting temperature (Tm) of the protein. The red and black vertical lines on the graph show the Tm of vCCI Y80A and vCCI WT, respectively. They are also tabulated in Table 3.1. The Tm of vCCI Y80A is 6.1°C lower than vCCI WT, indicating the point mutation significantly destabilizes the protein, though both are still quite stable, with melting temperatures above 70°C.

Table 3.1. Melting temperatures of vCCI WT and Y80A found by CD

Protein	Tm (°C)
vCCI WT	79.7 ± 0.6
vCCI Y80A	73.6 ± 0.2

I hypothesized that vCCI Y80A may actually stabilize the protein if the floppy acidic loop does indeed come down and make contacts with the β-sheets in the binding pocket. This hypothesis was proven wrong by the results of this experiment. It is really interesting that the CD spectra are so similar between the WT and mutant, but they have substantially different melting temperatures.

3.2 Nuclear Magnetic Resonance

3.2.1 Theory and Method

NMR stands for Nuclear Magnetic Resonance and uses radiofrequency to excite spins in magnetically active nuclei. Before excitation, the magnetic moments of the nuclei are randomly oriented. Nuclei with nuclear spin quantum numbers of I = ½, such as ^{1}H, ^{13}C, ^{15}N, and ^{31}P, are all commonly used in NMR because they have only 2 energy levels (given by 2I + 1).[23] This makes data less complicated to interpret. Of the nuclei listed, only ^{1}H and ^{31}P are naturally abundant. To isotopically label with ^{13}C and ^{15}N, the protein needs to be expressed with media where these isotopes are the sole source of the atom.

HSQC (Heteronuclear Single Quantum Coherence) spectra were collected. This technique relies on INEPT (Insensitive Nuclei Enhanced by Polarization Transfer) steps through J coupling, which allows for nuclear spin polarization transfer from H to another nucleus, usually to ^{13}C or ^{15}N (which the protein would need to be labelled with ahead of time).[24] In our case, ^{15}N labeling was used. The resulting spectra have axes of the chemical shift δ_H in ppm and the chemical shift of the other nucleus in ppm also. Each pair of a unique H bonded to the other nucleus is a peak on the spectrum. This is commonly referred to as a protein 'fingerprint'. Peaks shift differently based on their chemical environment, so if a protein is folded, distinct peaks should be seen. Chemical shifts are calculated as follows, with $vref$ corresponding to DSS:

$$\delta = \frac{(vobs - vref)}{vspect} * 10^6$$

NMR spectra were obtained on a 600 MHz Bruker Avance III spectrometer with four channels and a TCI cryoprobe. NMR experiments were done at 30°C and in a shaped tube to help reduce the noise from salt in the buffer. The buffer used was 20 mM NaPi, 100 mM NaCl, pH 7.0. Samples were prepared by adding 330 µL protein sample, 19 uL 99.8% D_2O, and 1.5 uL 5 mM DSS in D_2O.

3.2.2 Results and Discussion

Both vCCI WT and Y80A look folded due to distinct peaks above 9 ppm HN and low smearing down the middle of the spectra. The vCCI WT spectrum is very similar to known vCCI spectra and the vCCI Y80A spectrum overlays the WT spectrum nicely. It matches most peaks and only has some significantly shifted. These shifted peaks are key to understanding the difference in structure, which influences function. It is clear that the largest shifts (Y80A peak not touching the WT peak) are in I51, Y80, Y81, S82, I83, F92, G93, T95, K96, and S145 (not totally exhaustive). There are notable shifts (Y80A peak touching WT peak, but is offset from it) in V28, C97, S106, L139, E143, and V144 (not totally exhaustive). The NMR samples were only ^{15}N-labeled; to get better assignments, simultaneous ^{15}N- and ^{13}C-labeling is necessary. Some of the unassigned peaks moved substantially, but the identity of the peak was not known for certain.

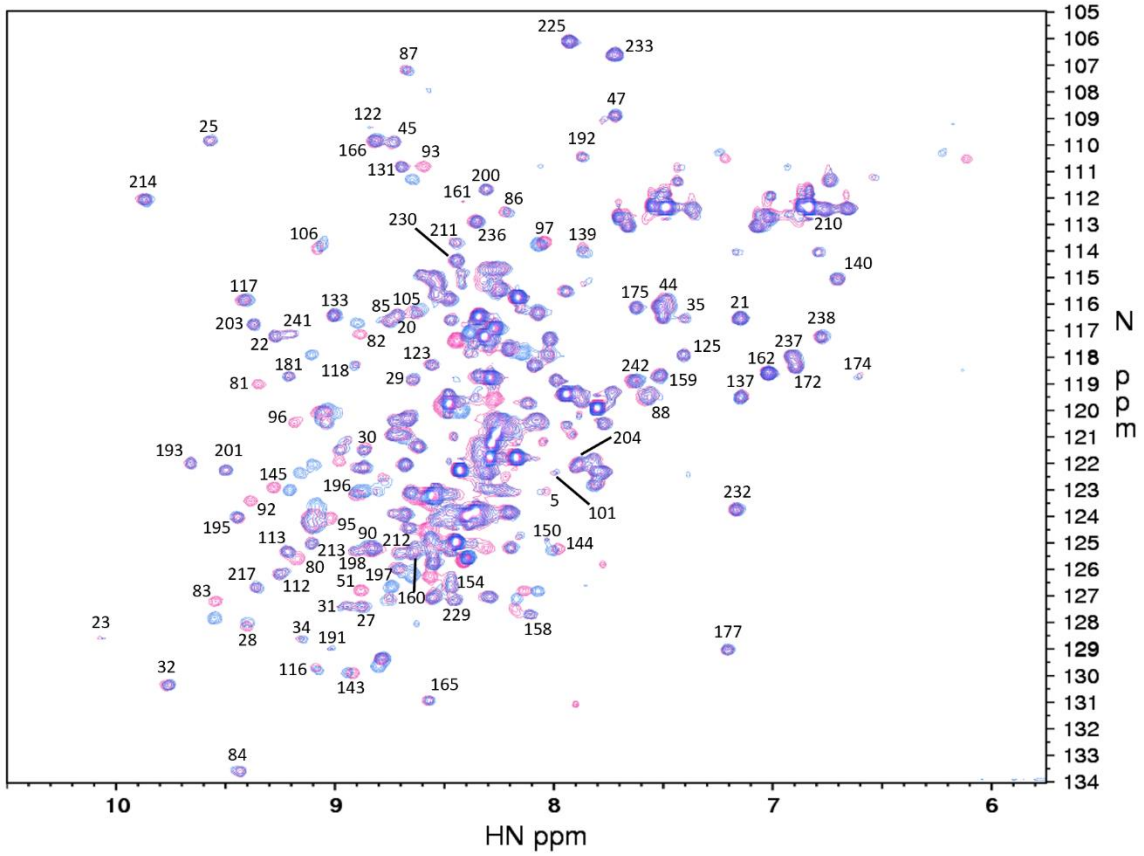

Figure 3.3. NMR HSQC spectrum of vCCI WT is shown in pink, with the HSQC spectrum of vCCI Y80A in blue overlaid on top. The colors combine when peaks overlap, making those areas purple. Many vCCI WT (pink) peaks are assigned, with the residue

number written next to peaks. The assignment data used to compare to these spectra can be found at BMRB: 6809. These are hard copy plots made in NMR Draw, then overlaid.

Figure 3.4. Residues that change chemical shift in the vCCI Y80A mutant mapped onto vCCI WT. vCCI WT (PDB 2FFK) is colored red. Residues that are highlighted in green have a moderate chemical shift perturbation (Y80A peak touching WT peak, but is offset from it) and yellow have a large chemical shift perturbation (Y80A peak not touching the WT peak), as evident in Figure 3.3, above. The figure was made using UCSF Chimera.[9]

The large (colored yellow) and moderate (colored green) shifts are mapped in Figure 3.4. It is to be expected that the residues right around the point mutation (such as 80-83) would have large shifts. However, some of these residues have also been found to shift substantially upon binding vMIP-II. The residues further away from Y80 in the sequence that shift are more interesting. The 90's and 140's regions are also known to shift a large amount upon vMIP-II binding.[18] It is supportive of our hypothesis that key binding residues on vCCI are shifting upon the Y80A mutation. This suggests that these residues are in a different environment, which could possibly be explained by a loop making contact with the β-sheets of the binding pocket.

3.3 Isothermal Calorimetry

3.3.1 Theory and Method

Isothermal calorimetry (ITC) is a useful tool for obtaining thermodynamic data of various interactions and functions by measuring the changes in heat as two molecules are titrated together.[25] The instrument has a reference cell and a sample cell. The cells are kept the same temperature through heating or cooling of the sample cell. The

instrument is very sensitive to changes in heat. The raw data is heat rate on the y-axis and time on the x-axis. Knowing the concentrations and volumes added allows the x-axis to be converted to mole ratio between the titrant and the titrand. The injection peaks areas are found through integration after the baseline and integration region are set and that becomes the new y-axis. A control is subtracted from the data, either by injection or by average area, to subtract out the heat from dilution. The remaining heat is from the interaction between the titrant and titrand. The data is fit and the result is what is known as a Wiseman Plot. The largest peak areas should be at the beginning of the titration and by the end of the titration, if the experiment is set up correctly, all the titrand should have reacted and the last few titrant injections should be just heat from dilution that will equal 0 after subtraction of the control. The change in heat between the beginning and end of the experiment gives you the change in enthalpy, modified to be per mole. The stoichiometric ratio (n) is found by the mole ratio when the transition from not fully bound to becoming fully bound occurs. The K_D is found from the slope of the transition.[26] A small K_D will have a large (steep) slope, whereas a large K_D will have a small (gradual) slope.

All ITC data was obtained on a TA Instruments Nano ITC Low Volume isothermal titration calorimeter. All experiments were done at 25°C with a stir rate of 350 rpm. The equilibration step before starting the experiment was set to 10 minutes (600 seconds). 20 injections, 2.5 µL each, of either 200 µM vCCI WT or 170 µM vCCI Y80A were titrated into 20 µM vMIP-II. All experiments were done in 20 mM NaPi, 100 mM NaCl, pH 7.0 buffer. The two controls and binding experiment for either vCCI WT or vCCI Y80A were all done on the same day to reduce variability.

The concentration of stock tubes of each protein was determined by the absorbance at 280 nm before starting experiments on a given day. The proteins were diluted to the desired concentration by mixing with the saved dialysis buffer, so there was no difference in buffers. To keep vMIP-II soluble, it had to be kept in 20 mM NaPi pH 2.5 buffer prior to dilution on the day of the experiment. The stock was very concentrated (1.3 mM) so only a few microliters of it was added to approximately 400 µL of the pH 7 buffer used in the experiment. The same ratio of 20 mM NaPi pH 2.5 buffer was added to all other solutions used in the experiment for minimal buffer mismatch. After dilution, the solutions were degassed for 20 minutes. While degassing, the ITC cells were rinsed 3 times with 400 µL of DI water. Once degassing was complete, the reference cell was rinsed 3 times with 300 µL of degassed DI water before being loaded with 300 µL DI water. This is only done for the first experiment of the day. Any proteins involved in the experiment had their absorbance taken immediately prior to loading into the cell or syringe to have the most accurate concentrations for data analysis. This is especially important for vMIP-II or other chemokines which are prone to aggregation at pH 7 buffer conditions.

The sample cell was rinsed 3 times with 300 µL degassed buffer before being loaded with 300 µL of either degassed buffer (for control) or vMIP-II (for control or binding experiment). The 50 µL titrating syringe was rinsed at least 3 times with degassed buffer before being loaded with either degassed buffer (for control) or degassed vCCI WT or Y80A (for control or binding experiment). The loaded titrating syringe was submerged into the sample cell and locked into place. The ‘Monitor’ tab on the ITC software was watched to see when the system reached equilibrium, then the stirring was engaged. Once the system reached equilibrium again, the experiment was

started. This two-step equilibration process was recommended to me by Colette Quinn at TA Instruments to be potentially useful when dealing with aggregating proteins.

After every experiment, the sample cell and syringes were washed with 1% Contrad-70 solution and rinsed with a lot of DI water. For the sample cell, 500 µL of the Contrad solution was added and pipetted up and down twice. Then, it was rinsed 10 times with 500 µL of DI water. After each of the first 5 washes, the loading syringe was rinsed an additional time with DI water to help remove Contrad from the syringe. After washing, the sample cell was left with 300 µL of DI water in it. The syringes were rinsed in a one-direction fashion by removing the plunger and spraying through the syringe with a DI water bottle for a minimum of 30 seconds.

3.3.2 Results and Discussion

The vCCI WT ITC data is shown in Figure 3.5 and modelled in Figure 3.6. The vCCI Y80A ITC data is shown in Figure 3.7 and modelled in Figure 3.8. Both show relatively tight binding to vMIP-II, with vCCI WT having a fitted K_D of 1.00×10^{-10} M (lower limit of detection) and vCCI Y80A having a fitted K_D of 2.99×10^{-8} M. For vCCI WT's K_D, we cannot say that it is 1.00×10^{-10} M, but we can say it is less than or equal to that value because the lower limit of detection of the ITC for K_D is 1.00×10^{-10} M. In all experiments involving vMIP-II, vMIP-II was in the sample cell. The vMIP-II concentration was kept constant at approximately 20 µM in all experiments with vMIP-II. In all experiments involving vCCI WT or vCCI Y80A, they were in the titrating syringe. The concentration of vCCI WT used in experiments was approximately 200 µM. The concentration of vCCI Y80A used in experiments was approximately 170 µM. The concentration of proteins was checked right before loading into the ITC for the most accurate experimental concentrations. There was some slight variability noted between experiments. I rounded all concentrations presented to the nearest µM value.

I would have liked to have done the experiments with the same concentration of vCCI WT and vCCI Y80A, but due to a slight logistical error, I had to do the vCCI Y80A experiment at a slightly lower concentration. Both experiments had all their controls done, which were internally consistent, and the vCCI WT and vCCI Y80A experiments were independent from each other. Because of this, the data is still interpretable, but the magnitudes of heat rates differ between the experiments (see the y-axis values in Figures 3.5 and 3.7). Note that the scales of Figures 3.5 and 3.7 differ for this reason.

The data presented below is a singlet of each binding experiment with two controls each. For vCCI WT and vCCI Y80A, the binding experiment and two controls were done on the same day to reduce variability as much as possible. The following 3 experiments were done for each vCCI (WT or Y80A):

- Binding experiment: vCCI titrated into vMIP-II
- vCCI control: vCCI titrated into buffer
- vMIP-II control: buffer titrated into vMIP-II

The legends of Figures 3.5 and 3.7 describe which curve corresponds to each experiment. In both cases, the black curve shows the vMIP-II control and the blue curve shows the vCCI control. For the vCCI WT experiment, the binding experiment data is shown in green. For the vCCI Y80A experiment, the binding experiment data is shown in red. In the upper graph of these figures, the 3 curves are stacked one on top of the other, so that each data set can be seen easily. Keep in mind that the baseline values

are not different between them (e.g. the corrected heat rate for the vMIP-II control in Figure 3.5 is not 1.5 µJ/s, it is actually 0 µJ/s). The curves are artificially stacked on top of each other for viewing ease. In the bottom graph of each figure, the curves are overlaid so it can be seen how much extra heat the binding experiment releases. The unobstructed green (for WT) and red (for vCCI Y80A) peaks for the first many injections show the heat change caused by binding events occurring. Later injections cause about as much heat as the vCCI controls, indicating no more binding events are occurring—all the vMIP-II has already been bound at that point.

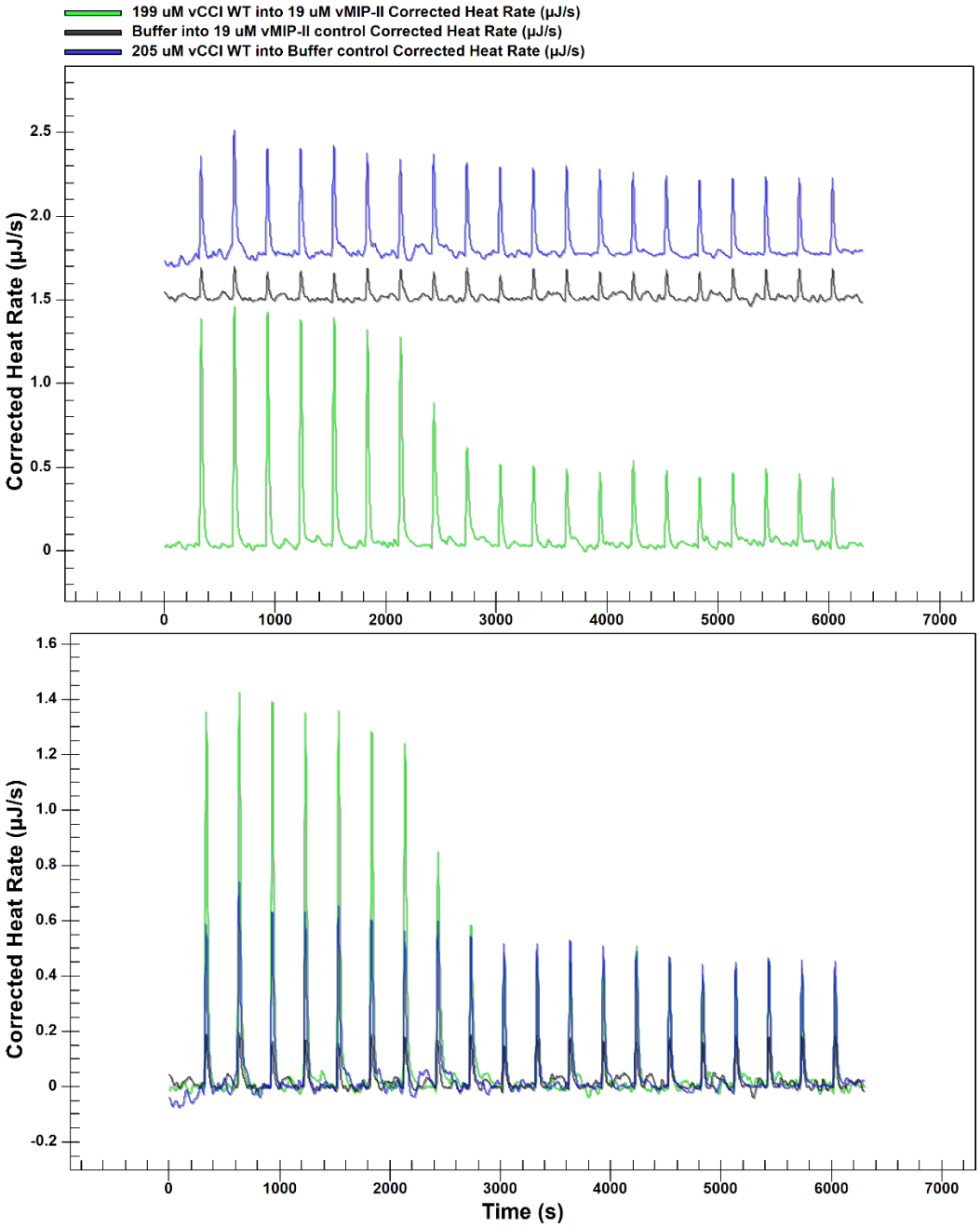

Figure 3.5. ITC corrected heat rates resulting from approximately 200 µM vCCI WT titrated into 20 µM vMIP-II. As described in the legend above, light green corresponds to

the binding experiment, blue is the vCCI WT into buffer control, and black is the buffer into vMIP-II control. The top graph shows the 3 experiments stacked on top of each other and the bottom graph shows them all overlaid.

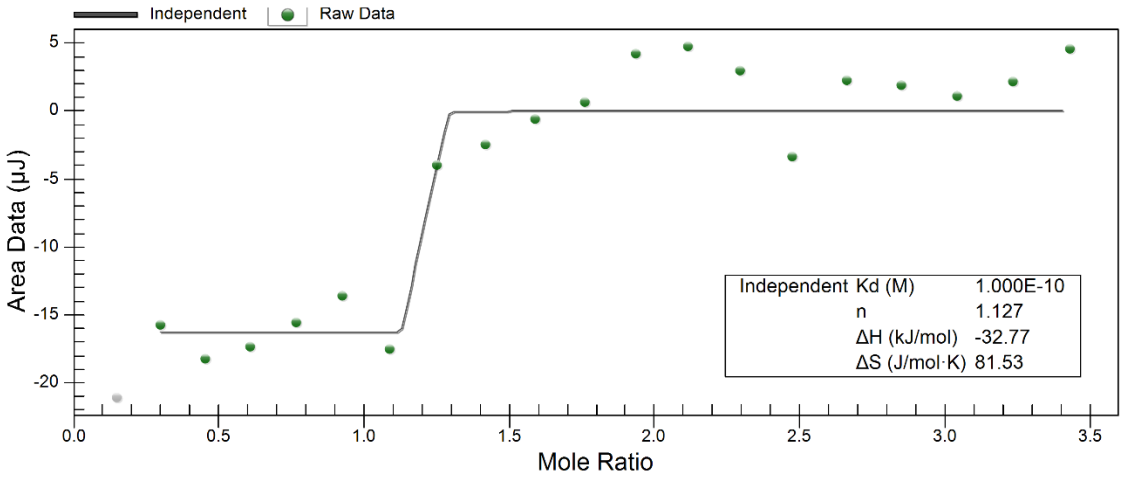

Figure 3.6. vCCI WT binding of vMIP-II modelled using the Independent model in NanoAnalyze. The binding experiment (light green) shown above had the vCCI WT into Buffer control (blue) subtracted out of it 'by injection'. The first data point was omitted from the fit, which is widely accepted and expected.

The vCCI WT binding experiment data was processed by manually fitting the baseline for each peak and selecting 125 second integration regions for injections 1-7, 100 seconds for injection 8, and then 80 seconds for injections 9-20. The vCCI WT control data was processed by keeping the automatically selected baseline and selecting 300 seconds as the integration region for all peaks. The control peak areas were subtracted from the binding experiment 'by injection'. Usually 'average area' subtractions are best, but this is only the case if the peak areas are staying constant throughout the control experiment. Subtraction 'by injection' was used because the control's peak areas had a small linear slope upward, which can be seen if there is a slight buffer mismatch. For this reason, the most accurate way to subtract the control from the experiment is to do it by injection because the injection peak areas are varying over the experiment in a small, but predictable way. The more one buffer is titrated into the other, the more similar they become. So, you will see there is some extra heat from mixing the buffers at the beginning and as they become more similar, the peak areas will decrease. The vCCI WT control was used instead of the vMIP-II control because it had a higher heat of dilution because it was more concentrated, and thus, it was a more appropriate control. Also, it can be seen to be a proper control by the fact that the later injections (already fully bound) average to about 0 after subtracting the control out (see Figure 3.6). This is what we would expect for a proper control.

The vCCI Y80A binding experiment data was processed by manually fitting the baseline and selecting 250 second integration regions for injections 1-8, 300 second integration regions for injections 9-14, and 150 second integration regions for injections 15-20. At first, the vCCI Y80A control was subtracted out, but its average peak area was a little more than the peak areas of the last few injections of the binding experiment, so it

was not the best control. Therefore, the average peak area of the last 5 injections of the binding experiment (-7.53 µJ) was subtracted from the data as the area correction. This is accepted in literature and in data processing protocols of test experiments for ITC.

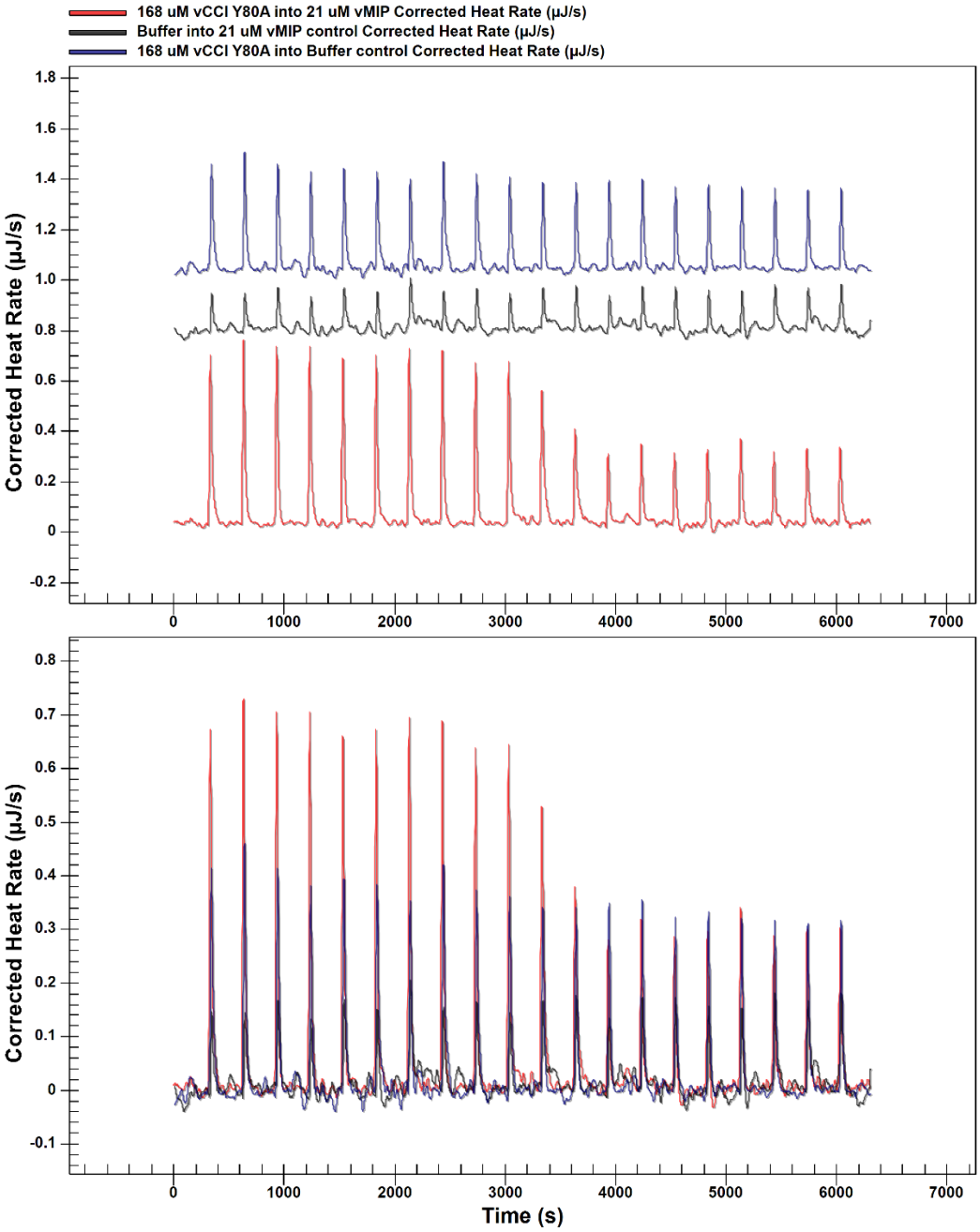

Figure 3.7. ITC corrected heat rates resulting from approximately 170 µM vCCI Y80A titrated into 20 µM vMIP-II. As described in the legend above, red corresponds to the binding experiment, blue is the vCCI Y80A into buffer control, and black is the buffer into vMIP-II control. The top graph shows the 3 experiments stacked on top of each other and the bottom graph shows them all overlaid.

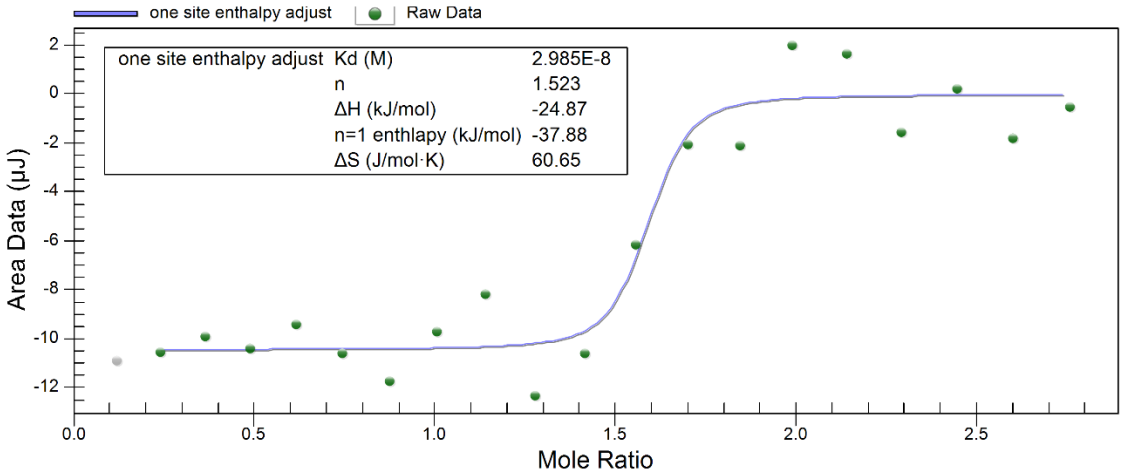

Figure 3.8. vCCI Y80A binding of vMIP-II modelled using the One Site Enthalpy Adjust model in NanoAnalyze, which is the same as the Independent model but also provides an additional adjusted enthalpy term for n=1, with nothing else changed. The binding experiment (red) shown above had its average area of injections 15 – 20 subtracted from itself. This is explained more in the text. The first data point was omitted from the fit, which is widely accepted and expected.

The stoichiometric ratios (n) for both complexes were close to 1, as expected. Also, the K_D for vCCI Y80A was higher than that for vCCI WT binding with vMIP-II, as we expected. Originally, I expected vCCI Y80A to have an even higher K_D than we saw from these experiments because it was shown to abolish function in the White, et al paper.[16] It is worth noting that the paper looked at how vCCI affected RANTES, not vMIP-II. I would expect RANTES to have an even higher K_D than vMIP-II for binding vCCI Y80A. Nevertheless, in thinking about the White, et al. results in light of my data, the K_D we obtained still makes sense with the loss of functionality they saw because of the concentrations they were using in their experiments. They incubated 5 nM RANTES with 15 nM vCCI Y80A for two hours before their experiment. K_D is the concentration of a ligand where it will be bound to half of its available binding partner. Given that we calculated the K_D of vCCI Y80A with vMIP-II to be 30 nM (and it is expected to be even higher for RANTES), then at equilibrium, very little of RANTES would have been bound by vCCI Y80A. Thus, if they changed their experimental concentrations to be higher, they would likely see some of vCCI Y80A's function, though it would be less potent than wild-type vCCI. Thus, our K_D is congruent with their results. The clear next steps are to repeat these experiments at the same concentrations as well as do binding experiments with RANTES to see if it has a significantly worse K_D with vCCI Y80A. While doing binding experiments with RANTES has been an issue due to aggregation in the past, the improved methods to reduce aggregation recently implemented should make it possible to get good data.

ITC is not ideal for complexes with K_D's this small because the concentrations needed for the experiment are much higher than the K_D, so all of the binding partner that is titrated in is immediately bound until all of the protein in the cell is fully bound, then smaller heat is released upon further addition of the binding partner because no

additional binding is occurring. This looks like a very quick transition between not fully bound and fully bound. You can tell from the data that it is tight binding and the data can be fit, but with the noise in the experiment, it makes it more difficult to feel confident that the K_D's are totally accurate. Repetition of the experiments and performing the experiments with the same concentration of vCCI WT and vCCI Y80A needs to be done to confirm the results seen in the singlet shown in this thesis. If the experiments were done near nM concentrations, one could also be confident, but there would not be enough signal above the noise to make sense of the data. For these reasons, fluorescence or SPR are good options for complexes with low K_D's. The ITC data we obtained was useful in giving us a close approximation of the K_D's and can be further bolstered by repeating the experiments but overall, fluorescence or SPR would be good techniques to use in the future.

Chapter 4

Conclusions and Future Directions

Overall, the experiments performed increased our knowledge about the vCCI Y80A mutant. Through CD, the melting temperature of vCCI Y80A was found to be 6.1°C lower than that of WT. The CD spectra at the beginning and end of the 25°C to 95°C temperature ramp were nearly identical. This suggests that the secondary structures at the beginning and end of the temperature ramp were very similar. Through NMR HSQCs, the changes in chemical shifts between unbound vCCI WT and vCCI Y80A were analyzed. The largest shifts were seen in residues in the early 50's, early 80's, early to mid 90's, and 145. Many of these residues have previously been determined to be important for vCCI binding.[10,11,18] This suggests that these residues are in different chemical environments, which supports our hypothesis that residues which are part of the binding pocket are in different locations than in WT vCCI.

The ITC results showed that both vCCI WT and vCCI Y80A are relatively tight binders, but vCCI Y80A has a larger K_D than vCCI WT. It was originally surprising that the K_D of vCCI Y80A with vMIP-II was found to be about 30 nM by ITC, but in looking back over the experimental set up by White, et al., it is congruent with their results.[16] Most of the RANTES in their pre-incubated mixture with vCCI Y80A would be free with a K_D of 30 nM or greater (for wild type vCCI, RANTES has a 4x higher K_D than vMIP-II) because they were using such low concentrations in their experiments. Thus, vCCI Y80A would not show much inhibitory effect.

The two main areas of focus going forward on this project are binding studies and NMR relaxation studies. For the binding studies, ITC will be used to repeat the experiments already done and to do RANTES binding. SPR and fluorescence will also be explored as options to obtain more accurate K_D values (because they are so low) and kinetic information. We predict that vCCI Y80A binding would have a slower on-rate, but a less- or non-affected off-rate. This is in contrast to what was seen for Y80R, which had an unaffected on-rate, but a faster off-rate.[17] This makes sense because R is bulky and could hold the loop open, but the positive charge was repulsive to the lysine on the chemokine.

NMR relaxation is a very promising way for us to test loop dynamics. vCCI Y80A will need to be assigned by ^{13}C, ^{15}N isotopic labeling of the protein. Then, NOE and CPMG experiments will be done to see if differences in relaxation of the loop region can be seen at nanosecond and micro- to millisecond time scales, respectively. Simulation data sees stable loop collapse for at least one microsecond. So, it will be great to test that experimentally via NMR. Also, we plan to obtain NMR HSQCs of labeled vCCI Y80A bound to non-labeled vMIP-II and labeled vMIP-II bound non-labeled vCCI Y80A.

Additionally, more mutants will need to be made to further test hypotheses generated by MD results, such as changes to the N-terminus (length or charge) and double mutants of Y80A and N-terminal alterations. MD simulations done by Lauren Stark suggest that the N-terminus length or charge could be helping to keep the loop open and have a partial rescue effect on binding for the Y80A mutant. The double mutants will help us test this. We hypothesize that a double mutant of Y80A and an N-terminal truncation or reduction of positive charge would have a higher K_D than vCCI with a sole Y80A mutation. We also plan to also investigate other poxvirus strains of

vCCI. For instance, mousepox has a shorter loop and we are interested in seeing how that affects binding and with comparable mutations to the N-terminus and Y80A in rabbitpox vCCI (which we have been using).

VII. References

1. Kufareva, I., Salanga, C. L. & Handel, T. M. Chemokine and chemokine receptor structure and interactions: implications for therapeutic strategies. *Immunol. Cell Biol.* **93,** 372–383 (2015).
2. Griffith, J. W., Sokol, C. L. & Luster, A. D. Chemokines and Chemokine Receptors: Positioning Cells for Host Defense and Immunity. *Annu. Rev. Immunol.* **32,** 659–702 (2014).
3. Gaertner, H. *et al.* Highly potent, fully recombinant anti-HIV chemokines: Reengineering a low-cost microbicide. *Proc. Natl. Acad. Sci.* **105,** 17706 LP-17711 (2008).
4. Abayev, M. *et al.* The solution structure of monomeric CCL5 in complex with a doubly sulfated N-terminal segment of CCR5. *FEBS J.* **285,** 1988–2003 (2018).
5. Bahar, M. W. *et al.* Structure and Function of A41, a Vaccinia Virus Chemokine Binding Protein. *PLOS Pathog.* **4,** e5 (2008).
6. Tortorella, D., Gewurz, B. E., Furman, M. H., Schust, D. J. & Ploegh, H. L. Viral Subversion of the Immune System. *Annu. Rev. Immunol.* **18,** 861–926 (2000).
7. Zhao, B. & Liwang, P. J. Characterization of the interactions of vMIP-II, and a dimeric variant of vMIP-II, with glycosaminoglycans. *Biochemistry* **49,** 7012–7022 (2010).
8. Liwang, A. C., Wang, Z. X., Sun, Y., Peiper, S. C. & Liwang, P. J. The solution structure of the anti-HIV chemokine vMIP-II. *Protein Sci.* **8,** 2270–80 (1999).
9. UCSF Chimera. Available at: http://www.rbvi.ucsf.edu/chimera/.
10. Zhang, L. *et al.* Solution structure of the complex between poxvirus-encoded CC chemokine inhibitor vCCI and human MIP-1beta. *Proc. Natl. Acad. Sci.* **103,** 13985–13990 (2006).
11. Kuo, N.-W. *et al.* Structural insights into the interaction between a potent anti-inflammatory protein, viral CC chemokine inhibitor (vCCI), and the human CC chemokine, Eotaxin-1. *J. Biol. Chem.* **289,** 6592–6603 (2014).
12. Burns, J. M., Dairaghi, D. J., Deitz, M., Tsang, M. & Schall, T. J. Comprehensive Mapping of Poxvirus vCCI Chemokine-binding Protein: EXPANDED RANGE OF LIGAND INTERACTIONS AND UNUSUAL DISSOCIATION KINETICS . *J. Biol. Chem.* **277,** 2785–2789 (2002).
13. Carfí, A., Smith, C. A., Smolak, P. J., McGrew, J. & Wiley, D. C. Structure of a soluble secreted chemokine inhibitor vCCI (p35) from cowpox virus. *Proc. Natl. Acad. Sci.* **96,** 12379 LP-12383 (1999).
14. Buatois, V. *et al.* Pan–CC Chemokine Neutralization Restricts Splenocyte Egress and Reduces Inflammation in a Model of Arthritis. *J. Immunol.* **185,** 2544 LP-2554 (2010).
15. Dabbagh, K. *et al.* Local Blockade of Allergic Airway Hyperreactivity and Inflammation by the Poxvirus-Derived Pan-CC-Chemokine Inhibitor vCCI. *J. Immunol.* **165,** 3418 LP-3422 (2000).
16. White, G. E., Mcneill, E., Christou, I., Channon, K. M. & Greaves, D. R. Site-Directed Mutagenesis of the CC Chemokine Binding Protein 35K-Fc Reveals Residues Essential for Activity and Mutations That Increase the Potency of CC Chemokine Blockade. *Mol. Pharmacol.* **80,** 328–336 (2011).
17. Arnold, P. L. & Fremont, D. H. Structural Determinants of Chemokine Binding by an Ectromelia Virus-Encoded Decoy Receptor. *J. Virol.* **80,** 7439–7449 (2006).
18. Nguyen, F. A. *et al.* Biophysical and Computational Studies of the vCCI:vMIP-II Complex. *International Journal of Molecular Sciences* **18,** (2017).

19. Beck, C. G. *et al.* The Viral CC Chemokine-binding Protein vCCI Inhibits Monocyte Chemoattractant Protein-1 Activity by Masking Its CCR2B-binding Site. *J. Biol. Chem.* **276,** 43270–43276 (2001).
20. Circular Dichroism. (2018). Available at: https://chem.libretexts.org/Textbook_Maps/Physical_and_Theoretical_Chemistry_Textbook_Maps/Supplemental_Modules_(Physical_and_Theoretical_Chemistry)/Spectroscopy/Electronic_Spectroscopy/Circular_Dichroism.
21. Greenfield, N. J. Using circular dichroism spectra to estimate protein secondary structure. *Nat. Protoc.* **1,** 2876–2890 (2006).
22. Greenfield, N. J. Using circular dichroism collected as a function of temperature to determine the thermodynamics of protein unfolding and binding interactions. *Nat. Protoc.* **1,** 2527–2535 (2006).
23. NMR: Introduction. (2017). Available at: https://chem.libretexts.org/Textbook_Maps/Physical_and_Theoretical_Chemistry_Textbook_Maps/Supplemental_Modules_(Physical_and_Theoretical_Chemistry)/Spectroscopy/Magnetic_Resonance_Spectroscopies/Nuclear_Magnetic_Resonance/Nuclear_Magnetic_Resonance_II.
24. Nguyen, F. A. Purification and Study of CC Chemokine-Based Strategies to Combat Chronic Inflammation and HIV. (University of California, Merced, 2017).
25. Duff Jr, M. R., Grubbs, J. & Howell, E. E. Isothermal titration calorimetry for measuring macromolecule-ligand affinity. *J. Vis. Exp.* 2796 (2011). doi:10.3791/2796
26. Wiseman, T., Williston, S., Brandts, J. F. & Lin, L.-N. Rapid measurement of binding constants and heats of binding using a new titration calorimeter. *Anal. Biochem.* **179,** 131–137 (1989).